CRN STRASBOURG

CRN 92-43

FOLDING MODEL ANALYSIS OF $^{58}Ni + ^{64}Ni$ ELASTIC AND INELASTIC SCATTERING AT E_{lab} = 203.8 AND 219.2 MeV

J.A. RUIZ and J.L. FERRERO
Instituto de Física Corpuscular, CSIC-Universidad de Valencia, Burjasot, Valencia, Spain

B. BILWES and R. BILWES
C.R.N. et Université Louis Pasteur, 67037 Strasbourg Cedex, France

CENTRE DE RECHERCHES NUCLEAIRES

STRASBOURG

IN2P3 CNRS

UNIVERSITE LOUIS PASTEUR

To be published in Nucl. Phys.

FOLDING MODEL ANALYSIS OF ^{58}Ni +^{64}Ni ELASTIC AND INELASTIC SCATTERING AT E_{lab} = 203.8 AND 219.2 MeV*

J. A. RUIZ and J. L. FERRERO

Instituto de Física Corpuscular, CSIC-Universidad de Valencia, Burjasot, Valencia, Spain

B. BILWES and R. BILWES[1]

Centre de Recherches Nucléaires and Université Louis Pasteur, Strasbourg, France

April 16, 1992

Abstract: Angular distributions of elastic scattering of ^{58}Ni by ^{64}Ni and inelastic scattering leading to the first 2^+ state in ^{58}Ni or in ^{64}Ni have been measured at E_{lab}=203.8 and 219.2 MeV. The data have been analyzed in the frame of the folding model. A renormalization N of the folding potential consistently lower than unity ($N\approx0.65$) is needed to reproduce the elastic scattering data. Coupled-channels calculations including the main inelastic channels explain partly this discrepancy. They reproduce the elastic and inelastic scattering data with a renormalization of $N\approx0.8$ at both energies. Interference between Coulomb and nuclear excitation is shown to play an important role in the repulsive character of the polarization potential.

NUCLEAR REACTIONS ^{64}Ni(^{58}Ni,^{58}Ni), E_{lab}=203.8,219.2 MeV, measured elastic and inelastic $\sigma(E,\theta)$. Folding model and coupled-channels analyses.

* Work partially supported by DGICYT (Spain) under project PB0415 1988/92 and by IN2P3-CNRS (France)

[1] deceased 17-1-91

1. Introduction

Elastic scattering and fusion of heavy ions at energies near the Coulomb barrier are two subjects that have generated a lot of interest in the last years. From the analysis of elastic scattering data of certain systems it was deduced a rapid increase (known as "threshold anomaly") of the nuclear attraction when the energy decreases approaching the Coulomb barrier [1-3]). On the other hand, at energies below the Coulomb barrier, the heavy ion fusion cross section of many systems is much greater than predicted by the conventional barrier penetration model [4-8]). It is obvious that both "anomalies" are related. However, while the threshold anomaly is unanimously ascribed to an effect of coupling to inelastic and transfer channels [1]), the description of the fusion anomaly is not so clear. Even recognizing the importance of coupling effects in this case, a variety of other models have also been proposed [4-10]). The experimental situation is quite different in both cases. The host of available sub-barrier fusion data, not only of light systems but also of medium and heavy ion projectile-target combinations contrasts with the scarcity of elastic scattering data measured at energies near the barrier. For this reason, the threshold anomaly has been studied only in a few systems, mainly light ones or using light projectiles [1]). Nevertheless, a detailed understanding of both anomalies and their mutual relationship requires as much information as possible for the studied systems. An experimental effort should be made to measure not only the fusion excitation function but also elastic and quasiclastic scattering at energies near the barrier, and, if possible, the fusion angular momentum distribution which is more sensitive to the mechanism underlying sub-barrier fusion than the excitation function alone (see for instance refs. [1,11,12])).

The surprising enhancement of sub-barrier fusion for ^{58}Ni+^{64}Ni and the differences observed with respect to ^{64}Ni+^{64}Ni and ^{58}Ni+^{58}Ni fusion justifies the great number of analyses dedicated to these systems [4-8]) even before any elastic or quasielastic measurements were available. Some years ago Rehm et al. [13]) measured the angular distributions of one nucleon transfer and elastic plus inelastic scattering in the interaction of ^{58}Ni+^{64}Ni at two energies. Only recently "pure" elastic angular distributions have been measured by Stefanini and collaborators [14]), but no inelastic data were available until now. In the present paper we report our measurement of the

angular distributions of the elastic and inelastic scattering of ^{58}Ni on ^{64}Ni at E_{lab} = 203.8 and 219.2 MeV, which corresponds approximately to 9 MeV and 17 MeV above the Coulomb barrier in the centre of mass system ($V_{CB} \simeq 98$ MeV-CM). Our lower energy matches the upper of refs. [13,14]) in order to check our data. The experimental method is summarized in section 2. In section 3 the elastic scattering is analysed using the folding model. In section 4 we study the coupling between elastic and inelastic channels in the framework of the folding model. Finally we discuss the results and give the conclusions of this work in section 5.

2. Experimental method

The experiment was performed at the MP tandem of the CRN at Strasbourg. The target was obtained by evaporating $\simeq$20 μg/cm^2 of enriched (93%) ^{64}Ni on a $\simeq$20 μg/cm^2 carbon foil. Two position sensitive silicon detectors (48 x 9 mm^2) were placed at 240 mm from the target, one on each side of the beam, at angles chosen so that the maximum efficiency was achieved for detection in coincidence of the ejectile and residual nucleus from quasielastic reactions. The silicon detectors give the energies and the scattering angles of the two nuclei in the laboratory frame; from this, their mass, scattering angle θ_{CM} in the centre of mass and Q-value of the reaction can be easily obtained. The events corresponding to a particular exit channel partition are characterized by their calculated masses $m_{1,2}$ lying around the expected masses. In that form we can separate transfer reactions from elastic and inelastic scattering as it has been shown in many previous experiments with sd-shell nuclei [15,16]).

In figure 1 we show a mass spectrum obtained for a detector configuration which presents the maximum yield in the transfer of one and two nucleons. We observe that the peak centred at $m_1 = 58$ and $m_2 = 64$, corresponding to elastic and inelastic scattering events, has a FWHM $\simeq$ 1.0 a.m.u. which is rather small but large enough to contaminate appreciably the events of one and two nucleon transfers which should be placed around the pointed crosses in the figure. Figure 2 shows Q-spectra for two kind of events. In the upper histogram, obtained with the whole set of events in fig. 1, we see the peak of elastic scattering (Q around zero) with FWHM $\simeq$ 900 KeV which is clearly separated from a second peak around $Q = -1.4$ MeV corresponding to the inelastic excitation of ^{58}Ni(2^+,1.45) or ^{64}Ni(2^+,1.34). Inelastic scattering to higher levels is

not resolved. The contamination due to transfer reactions in elastic and 2^+ inelastic scattering is negligible (10% at most) because of the comparatively low yield of transfers as can be seen in the lower histogram of figure 2 which has been obtained with the events within the dashed contour in fig. 1. This Q-spectrum is similar to the one obtained by Rehm and collaborators [13]) who achieved a better mass resolution. The angular distributions obtained from spectra like figure 2, are centred at the same angle and have a similar form as those shown in ref. [13]). This confirms that most of the events in the dashed rectangle of figure 1 are those of the transfer of one nucleon. The contamination due to elastic and inelastic scattering in the transfer peak is difficult to evaluate but probably important, especially for $Q > -2$ MeV. For this reason we did not analyse the transfer angular distributions. Nevertheless we should mention that a better mass resolution can be obtained using a thinner target to avoid energy straggling of the reaction products. So it may be possible in a near future to measure also transfer reactions with our simple set up. We are currently working on this purpose.

Four different set of angles of the detectors were enough to measure the whole angular distributions. In each configuration about twenty points were obtained simultaneously. The various configurations were chosen so that a considerable overlap allowed the normalization between the different parts. Absolute values of cross sections were obtained by normalizing to the Rutherford scattering the experimental elastic plus inelastic scattering ($Q > -5$ MeV) at the most forward angles. This permits to take into account that the strong Coulomb excitation of the low-lying 2^+ states deviates the elastic angular distribution from Rutherford even at the most forward angles ($\theta_{CM} \simeq 50°$) we have measured. As it is shown in ref. [17]) at these smaller angles the sum of the elastic and inelastic cross sections is almost exactly equal to the Rutherford cross section. We believe that the absolute values are correct to a 5%. The measured angular distributions are presented in the next sections. The error bars include the statistical error plus the relative normalization errors between the different configurations.

In order to test our experimental set up in this relatively heavy system we compare in figure 3 our measurements of the elastic scattering cross section at 203.8 MeV and the sum of it and the inelastic scattering to the first levels of ^{58}Ni and ^{64}Ni ($Q > -5$ MeV) with two available previous

measurements. The results of Rehm et al. [13]) were obtained with a magnetic spectrograph and those of Stefanini et al. [14]) with a modified version of the kinematical coincidence method. Both results coincide with our summed curve. In ref. [13]) it is said that the points include elastic and inelastic scattering to low-lying states. On the contrary in ref. [14]) it is claimed that pure elastic scattering has been measured. We conclude that there is a disagreement between our pure elastic curve and the result of the Legnaro group (our curve is lower by 20 % to 50 % for $\theta_{CM} > 90°$).

3. Elastic scattering analysis with the folding model

The folding model permits a more coherent and unambiguous analysis of experimental data than phenomenological potentials. In particular, when used with the M3Y effective nucleon-nucleon interaction of Bertsch et al. [18]) it has demonstrated to give the "bare" real optical potential (i.e. without polarization term) within 10 % of uncertainty or better in a great number of systems [19]). Therefore this model provides a good basis to the analysis of the present measurement, which in turn constitutes a further test of the model. The optical potential is

$$V_{opt}(r) = NV_F(r) + V_C(r) + iW(r) \tag{1}$$

where the real nuclear part is given by the folding integral

$$V_F(r) = \int\int \rho_1(r_1)\rho_2(r_2)v(|\mathbf{r}_1 - \mathbf{r}_2 + \mathbf{r}|)\mathrm{d}\mathbf{r}_1\mathrm{d}\mathbf{r}_2 \tag{2}$$

The densities $\rho_i(r)$ are the sum of the proton and neutron point nuclear densities and were taken from ref. [20]) in which they were extracted from the scattering of 0.8 GeV polarized protons. The effective nucleon-nucleon interaction $v(r)$ we used is the above mentioned M3Y and the integral (2) was evaluated with the DFPOT code [21]). The Coulomb potential $V_C(r)$ was calculated by folding the proton densities with the Coulomb interaction and for the imaginary potential $W(r)$ we took a standard Woods-Saxon shape. The renormalization factor N was left as a free parameter as well as the radius R_W and the diffusivity a_W of the imaginary potential. The imaginary depth was fixed to $W = 50.0$ MeV in order to ensure total absorption at small distances. In that case the particular value of W is not important as only the potential in the surface determines the scattering. We introduced V_{opt} into the ECIS code [22]) which searches

automatically the value of the free parameters that minimize the χ^2 of the fit, defined as usual. The results are reported in the table and the corresponding fits are presented in figure 4 (long dashed lines) in a linear scale. The errors given for the N parameter indicate the range of variation of N which produces an increase of χ^2 by less than a 10% of the minimum. As it is well known a change in the value of a_W can generally be compensated with a variation of R_W so that χ^2 remains constant. This means that there exists a family of potentials that give the same quality of fit. These potentials cross each other approximately at a point $R_s(W)$ that we identify as a "sensitivity radius" where the potential is best determined by the data and which is reported in the table. The same procedure can be used to determine a sensitivity radius for the real potential $R_s(V)$; for this purpose we substituted the folding potential for a Woods-Saxon potential which reproduces accurately the folding in the region $r > 8$ fm.

As it is shown in the table, very low values of N are obtained at both energies. Moreover although the χ^2 values per point are not high it is clear from the figure that the fits do not reproduce the rainbow angular region ($\theta_{CM} < 80°$). By analogy to what was already observed in other systems the poor fit of this region can be ascribed to the strong Coulomb excitation of low-lying levels of the projectile and the target [17]). The large diffusivities of the imaginary potentials obtained by fitting the data (see table) may in fact simulate partly the effect of the Coulomb excitation but it is unclear if the surprisingly low values obtained for N attempt also to simulate this effect or are due to effects not taken into account in the folding model.

The Coulomb excitation of low-lying levels in heavy-ion collisions can be represented by a polarization potential which is believed to be mainly imaginary. In the sudden limit, for example, this potential has a negligible real part while the imaginary part behaves as $\sim 1/r^5$ at large distances [17]). Our idea was to introduce explicitly such a long range imaginary potential and, by fitting the data, to see if it was possible to restore the adequacy of the folding model. For simplicity we added to the volume imaginary potential a surface term with a Woods-Saxon derivative form whose parameters, together with the previous three parameters, were varied in order to fit the elastic scattering data. The parameters that minimize χ^2 are given in the table, they correspond to relatively good fits (see short-dashed curves in figure 4). At the higher energy

the theoretical curve is still unable to reproduce the oscillations in the experimental data at angles lower than 80 degrees. The parameters of the table show that the surface imaginary term is quite small and it is placed at very large distances where the volume term is negligible. The inclusion of a surface absorption has the effect to reduce the volume imaginary potential diffusivity but it has not an appreciable influence on the renormalization factor, which remains very small ($N \approx 0.65$ at both energies). We verified that this result does not depend on the experimental data normalization, changing it by a 10% implies variations of less than a 5% in the N value given in the table.

In preceding folding analyses of elastic scattering between heavy ions near the Coulomb barrier the N factor was always found equal or greater than unity [19]). The deviations from the M3Y folding potential were attributed to an attractive real polarization potential due to the coupling between elastic and quasielastic channels. The present result seems to indicate that in this system such a coupling generates an important real polarization potential which is not attractive but repulsive. To clarify this point we pursued the calculations by coupling explicitly the most important inelastic channels to the elastic one.

4. Coupled-Channels Analysis

In the framework of the folding model, the real potential to be used in the coupled equations is given by the usual folding formula (2) with the densities of ^{58}Ni and ^{64}Ni deformed according to the presence of the 2^+ levels, which are taken as quadrupole vibrations of the nuclei. Up to second order the point nuclear density for each nucleus reads [23])

$$\rho(\mathrm{r},\alpha) = \rho(r) - r\frac{\mathrm{d}\rho(r)}{\mathrm{d}r}\sum_{\mu}\alpha_{2\mu}Y_2^{\mu}(\theta,\phi)^* + \frac{1}{2}\sum_{\lambda\mu}(r^2\frac{\mathrm{d}^2\rho(r)}{\mathrm{d}r^2} + 4r\frac{\mathrm{d}\rho(r)}{\mathrm{d}r}\delta_{\lambda 0})\frac{\hat{2}\hat{2}}{\sqrt{4\pi}\hat{\lambda}} < 2200|\lambda 0 > [\alpha_2 \times \alpha_2]_{\lambda\mu}Y_{\lambda}^{\mu}(\theta,\phi)^* \quad (3)$$

where $\alpha_{2\mu}$ are the deformation parameters. The factor $\delta_{\lambda 0}$ in the last term is necessary in order to conserve the number of nucleons. Inserting this expression into the folding formula (2) the central potential and the different coupling potentials are obtained again as folding integrals; the only difference is that for the coupling potentials one or both densities $\rho_i(r)$ are replaced by

derivatives of the densities. These integrals were calculated by means of the DFPOT code. The "bare" densities to be used in (3) are obtained from the experimental ones of ref. [20]) by the relation

$$\rho_{exp}(r) \equiv < 0|\rho(r,\alpha)|0 > \\ = \rho(r) + \frac{1}{2}\frac{\beta_N^2}{4\pi}(r^2\frac{d^2\rho(r)}{dr^2} + 4r\frac{d\rho(r)}{dr}) \quad (4)$$

This second order differential equation can be easily resolved by numerical integration. The values for the nuclear deformation β_N were taken equal to the Coulomb ones β_C deduced from the experimental B(E2). As there exists a certain dispersion in the values given in the literature [24-26]), we chose B(E2↑,^{58}Ni)=660 e^{2}fm^4 and B(E2↑,^{64}Ni)=650 e^{2}fm^4 from ref. [27]) which gave good results in preliminary calculations. The Coulomb coupling potentials were calculated, mutatis mutandis, in the same way. For the imaginary potential we used a standard Woods-Saxon form with the depth fixed at $W = 50.0$ MeV and deformed to second order in the usual prescription. The deformation parameter for the imaginary potential was taken as a half of β_N following the idea that the deformation lengths for the potential and the density are equal and given that the system is quasisymmetric. The resulting coupling potentials and the bare potential were supplied to the coupled channels code ECIS in order to resolve the coupled equations. As in the one channel case, the real potential and couplings were multiplied by a renormalization factor N which was varied, together with the imaginary radius and diffusivity, in order to minimize χ^2. The best fits obtained are presented in figure 4 (full lines) in linear scale, and in figure 5 (full lines) in logarithmic scale. The corresponding parameters are presented in the table.

As can be seen in figure 4 the fit of the lower angles (rainbow region $\theta_{CM} < 80°$) is qualitatively much better than the one obtained considering only the elastic channel. At larger angles ($\theta_{CM} > 90°$) and at both energies the theoretical curve presents oscillations which are superimposed on a normal smooth behaviour as is shown in figure 5. The experimental curves show also small oscillations although somewhat shifted with respect to the theoretical ones. In figure 5 are also presented the angular distributions for the excitation of the first 2^+ level of ^{58}Ni or ^{64}Ni at both energies which are rather well fitted, although somewhat overestimated at intermediate angles. In this case the theoretical curve does not present oscillations. As expected, the effect on the potential of the coupling to the 2^+ levels is to reduce drastically the diffusivity of the

imaginary potential (see table) but also supposes an increase of the renormalization factor N, which for the higher energy reaches the value $N = 1$. This supports the idea that the low N value obtained in the one channel case is due to the effect of the inelastic excitation. The role of the Coulomb excitation can be investigated by performing coupled-channel calculations with only Coulomb coupling. In that case the best fit of the elastic scattering data is obtained with a renormalization of $N = 0.50$ for 203.8 MeV and of $N = 0.88$ for 219.2 MeV. At the lower energy N diminishes when the Coulomb coupling is switched on (compare with the table). Therefore the polarization potential produced by this coupling alone is attractive at this energy but it becomes repulsive when the nuclear and imaginary couplings are also switched on as N increases in this case. On the contrary, for the higher energy the polarization potential produced by the Coulomb coupling alone is already repulsive and becomes still more repulsive when the other couplings are included. The effect of the Coulomb coupling alone on the N value is a little puzzling but it is clear that the final value of N in the table relies on the interference between nuclear and Coulomb excitation.

It is interesting to note that the inelastic scattering data cannot be reproduced without the imaginary part of the coupling (see fig. 5, point-dashed curve). This means that these levels are excited also by multistep processes. In ref. [28]) a theoretical investigation of the imaginary form factor leads to the conclusion that its long range part is governed by transfer reactions. In the present system, neutron transfer channels are very important. They have a total yield comparable to the excitation of one of the 2_1^+ levels ($\sim$ 200 mb). Therefore such transfer channels may be responsible for the imaginary coupling observed and could play a predominant role in fusion, as suggested by Stelson [29]). Note that the imaginary sensitivity radius $R_s(W)$ is placed at $\simeq$ 1 fm outer than the real one $R_s(V)$. This can be related either to the strong Coulomb excitation or to the important neutron transfer reactions. We believe that the second reason is more plausible. At the position of $R_s(W) = 12.0$ fm the imaginary potential generated by the Coulomb excitation is probably small compared with the whole imaginary potential. On the other hand just at these distances the flow of neutrons from ^{64}Ni to ^{58}Ni start to be possible [29]). In order to see the relative importance of the different parts of the coupling we show in fig. 6 a decomposition of the cross section at $E_{lab} = 203.8$ MeV. The inelastic scattering is dominated by

the Coulomb coupling as well as elastic scattering up to $\theta_{CM} \simeq 100°$. The nuclear and imaginary couplings determine the slope of the fall in both angular distributions. The interference between the Coulomb and nuclear couplings is destructive while it is constructive between the Coulomb and imaginary ones. This permits to fit the larger angles with help of the imaginary excitation.

In order to evaluate the effect on the optical potential of the coupling to higher levels we have included explicitly in the coupled channels the mutual excitation of the first 2^+ levels and the excitation of the first 4^+ levels of both nuclei, ^{58}Ni(4^+, 2.46 MeV) and ^{64}Ni(4^+, 2.61 MeV), which where taken as two phonon states. The best fit parameters are reported in the table and the corresponding fits are shown in figure 5 (dashed lines). At intermediate angles the 2^+ inelastic distribution is better reproduced than in the two channel calculation. The effect on the imaginary potential is not important (see table) because these channels do not absorb a lot of flux as in the case of the 2^+ levels. On the contrary there is a sizeable reduction of the N value for the higher energy. In the end we obtain $N \approx 0.8$ at both energies. We repeated the calculations taking the 4^+ levels as one phonon states, as there is experimental evidence on this from α+^{58,64}Ni scattering [30]). We obtained essentially the same results for the renormalization N. In fact the yield of the 4^+ levels is much lower that the mutual 2^+ excitation yield, and they have little influence on the N value. Taking this into account, we think that the effect on N of a single higher level excitation will not be important, but the combined effect of the many levels excited at $Q < -3$ MeV may be considerable. The same could be said about the one and two neutron transfer reactions.

So, after having taken into account the main inelastic channels the N factor is somewhat low with respect to the "expected" value $N = 1$. It could be that a small error in the point nuclear densities used would explain this discrepancy. But given that, as it has been seen, the influence on N of the coupling to inelastic channels is important (and rather unpredictable), it should be natural to pursue the analysis by including explicitly in the calculation the excitation of higher-lying levels and transfer reactions. Unfortunately this is difficult because the coupling scheme gets very complicated when all those channels are included in the calculation. Moreover the correct inclusion of transfer reactions, which have an important yield in this system, increases

greatly the number of channels and requires the solution of coupled integral-differential equations. For this reason we did not attempt such an analysis in the present work which, anyway, has more restricted objectives. Extensive calculations of this kind have been done only in very few cases either exactly or making approximations (see ref. [11]) and references therein).

5. Discussion and conclusions

The precise measurement of elastic scattering of ^{58}Ni on ^{64}Ni and inelastic scattering leading to the first 2^+ state in ^{58}Ni or in ^{64}Ni have been performed at two energies slightly above the Coulomb barrier. An acceptable reproduction of the elastic scattering data in the framework of the folding model requires the inclusion of a long range absorptive potential and the renormalization of the folding potential by a factor $N \approx 0.65$ at both energies. Renormalizations significantly lower than unity have been found in analyses with the folding model of d,t,^{3}He,^{6,7}Li and ^{9}Be scattering [19,31–34]) and they have been related to the breakup of these low bound nuclei. Such a kind of renormalization is necessary also to describe elastic scattering of rather bound systems at high energies [35,36]). In that case the opening of the breakup channels or the possible fail of the M3Y effective interaction at these high energies could be responsible for this effect. Nevertheless, the M3Y interaction has proved to be adequate at energies near the Coulomb barrier. As far as we know, this is the first time that an important reduction of the folding potential is necessary in this energy domain for a bound (heavy) system like this.

Our interpretation is that the coupling to the quasielastic channels generates a significant polarization potential which is repulsive at the studied energies. This is supported by explicit coupled-channels calculations. Including the excitation of the first 2^+ levels in ^{58}Ni and ^{64}Ni makes unnecessary the renormalization of the potential at 219.2 MeV and diminishes the reduction of the potential to $N = 0.83$ at 203.8 MeV.

Nevertheless, a renormalization of $N \approx 0.8$ is still necessary at both energies when including the excitation of the first 2^+ and 4^+ states of the projectile and the target as well as the mutual 2^+ excitation in the coupled channels. It is reasonable to attribute this rather low N value to the effect of the coupling to other important reactions as the inelastic excitation of levels at

$Q < -3$ MeV and one and two neutron transfer reactions. This is supported by the successful coupled-channels calculations of ref. [11,14]). In that work Esbensen and Landowne have performed calculations in a coupled-channel formalism which include, with some approximations, the main inelastic and transfer channels. They use a Woods-Saxon real potential which coincides with our folding potential at radii $r > 10$ fm. Then we can consider that they use as bare potential the M3Y-folding one. Although they deform directly the potentials and not the densities as in the folding model, which is in principle more correct, it may well be that both procedures give similar results. It is encouraging to observe that such a complicated calculation can reproduce rather well the elastic scattering measured by the Legnaro group at 203 and 189.6 MeV and the fusion excitation function. In fact the theoretical prediction fits better our data at 203.8 MeV than that of reference [14]) (see fig. 3 and compare with fig. 2 of ref. [14])). It is interesting to note that the real part of the polarization potential produced by the couplings in the calculation, for zero total angular momentum and at the position of the Coulomb barrier, is positive (i.e. repulsive) at energies greater than the barrier (see fig. 8 in ref. [11])). This effect is confirmed in the present work where the repulsive nature of the polarization potential is deduced from the analysis of the elastic scattering data. We have shown that the Coulomb excitation plays an important role in this repulsive character, in particular through the interference with the nuclear excitation. The importance of this interference on the partial fusion cross section of ^{58}Ni+^{58}Ni is stressed by Landowne and Pieper [37]).

A related subject is the possibility to determine the optical potential energy dependence from the elastic scattering data. It is well known [1]) that the polarization potential can change its form with the energy near the barrier. Therefore the renormalization N of the folding potential gives only the approximate optical potential values near the sensitivity radius while it says little about the form of the potential at closer distances. In the present system the sensitivity radius for the real part $R_s(V)$ is placed at greater distances than the barrier ($r_{CB} \approx 10.2$ fm for $N = 0.65$). In fact this renders difficult the determination of the Coulomb barrier height from the elastic scattering alone. Moreover the sensitivity radius for the imaginary part $R_s(W)$ does not coincide with $R_s(V)$. This would make difficult the application of the dispersion relation to the study of the threshold anomaly in this system.

These difficulties can be tackled with more precise elastic scattering measurements at energies near the barrier and it is clear that inelastic scattering and transfer data would be very valuable. Analysis of such data requires the use of the coupled-channels approximation. Hence, we are led to a description of the main reaction processes simultaneously in a coupled-channel approach like that confronted in ref. [11]). However such an approach would not be possible in very heavy-ion systems, which present a lot of important quasielastic channels. For this reason an alternative (more macroscopic) description is still necessary for them, like the modified barrier penetration model recently proposed [38]), or a more sophisticated one. Therefore, the study of intermediate systems like Ni+Ni by means of the coupled channels would help to obtain a better understanding of the physical meaning of quantities and concepts introduced in macroscopic models.

In conclusion, we have seen that coupling between various inelastic channels are important in the scattering of ^{58}Ni+^{64}Ni at 203.8 and 219.2 MeV, and its importance would possibly increase when the energy approaches the Coulomb barrier. Inelastic scattering data has proved to be valuable in order to reduce the uncertainties in the determination of the optical potential, therefore it would be of great interest to continue such measurements at lower energies and extend them to transfer reactions.

The authors wish to express their gratitude to L. Stuttge for her participation to the measurements and for the careful reading of the manuscript and to J. C. Pacheco for stimulating discussions.

References

1) G. R. Satchler, Phys. Reports **199** (1991) 147

2) C. Mahaux, H. Ngô and G. R. Satchler, Nucl. Phys. A449 (1986) 354

3) M. A. Nagarajan, C. Mahaux and G. R. Satchler, Phys. Rev. Lett. **54** (1985) 1136

4) M. Beckerman, Rep. Prog. Phys. **51** (1988) 1047

5) S. G. Steadman and M. J. Rhoades-Brown, Ann. Rev. Nucl. Sci. **36** (1986) 649

6) P. Armbruster ed., *Proc. Argonne Symp. on the Many Faces of Heavy Ion Fusion Reactions* ANL-PHY-86-1

7) S. C. Steadman, ed. *Fusion reactions below the Coulomb Barrier*, Lecture Notes in Physics, vol. 219 (Springer, Berlin, 1985)

8) M. Beckerman, Phys. Reports **129** (1985) 145

9) C. Signorini, S. Skorka, P. Spolaore and A. Vitturi eds., *Heavy Ion Interactions Around the Coulomb Barrier*, Lecture Notes in Physics, vol. 317 (Springer, Berlin, 1988)

10) M. A. Nagarajan ed., *Heavy Ion Collisions at Energies Near the Coulomb Barrier*, Institute of Phys. Conference Series, vol. 110 (Galliard, Norfolk, 1991)

11) H. Esbensen and S. Landowne, Nucl. Phys. A492 (1989) 473

12) M. L. Halbert, J. R. Beene, D. C. Hensley, K. Honkanen, T. M. Semkow, V. Abenante, D. G. Sarantites and Z. Li, Phys. Rev. C40 (1989) 2558

13) K. E. Rehm, F. L. H. Wolfs, A. M. van der Berg and W. Henning, Phys. Rev. Lett. **55** (1985) 280

14) A. M. Stefanini, Xu Jincheng, L. Corradi, G. Montagnoli, H. Moreno, Y. Nagashima, L. Mueller, M. Narayansamy, D. R. Napoli, P. Spolaore, S. Beghini, F. Scarlassara, G. F. Segato, F. Soramel, C. Signorini, H. Esbensen, S. Landowne and G. Pollarolo, Phys. Lett. B240 (1990) 306

15) J. A. Ruiz, Thesis, University of Valencia, (unpublished)

16) B. Bilwes, R. Bilwes, V. D'Amico, J. L. Ferrero, R. Potenza and G. Giardina, Nucl. Phys. A408 (1983) 173

17) W. G. Love, T. Terasawa and G. R. Satchler, Nucl. Phys. A291 (1977) 183

18) G. Bertsch, J. Borysowicz, H. McManus and W. G. Love, Nucl. Phys. A284 (1977) 399

19) G. R. Satchler and W. G. Love, Phys. Reports 55 (1979) 183

20) G. W. Hoffmann, G. S. Blanpied, W. R. Coker, C. Harvey, R. P. Liljestrand, G. S. Adams, T. S. Bauer, G. Igo, G. Pauletta, C. A. Whitten Jr., A. Wreikat, L. Ray, J. E. Spencer, H. A. Thiessen, H. Nann, K. K. Seth, N. M. Hintz, G. Kyle, M. A. Oothoudt, B. E. Wood, D. K. McDaniels, C. Glashausser and M. Gazzaly, Phys. Lett. B79 (1978) 376

21) J. Cook, Comp. Phys. Comm. 25 (1982) 125

22) J. Raynal, Phys. Rev. C23 (1981) 2571

23) G. R. Satchler, *Direct Nuclear Reactions*, (Oxford Univ. Press, Oxford, 1983)

24) L. K. Peker, Nuclear Data Sheets 42 (1984) 457

25) P. M. Endt, At. Data Nucl. Data Tables 23 (1979) 547

26) M. Beckerman, R. L. Auble, F. E. Bertrand, J. L. Blankeship, B. L. Burks, M. A. G. Fernandes, C. W. Glover, E. E. Gross, D. J. Horen, R. O. Sayer, G. R. Satchler, D. Shapira, Y. Sugiyama and R. L. Varner, Phys. Rev. C36 (1987) 657

27) F. Videvaek, P. R. Christersen, Ole Hansen and K. Ulbak, Nucl. Phys. A256 (1976) 301

28) C. H. Dasso, G. Pollarolo and S. Landowne, Nucl. Phys, A443 (1985) 365

29) P. H. Stelson, Phys Lett. 205B (1988) 190

30) F. Ballester, E. Casal, J. Diaz, J. B. A. Englend and F. Moriano, J. Phys. G: Nucl. Phys. 13 (1987) 1541

31) J. Cook and R. J. Griffiths, Nucl Phys. A366 (1981) 27

32) J. Cook, Nucl. Phys. A375 (1982) 238

33) J. Cook, Nucl. Phys. A382 (1982) 61

34) C. L. Woods, B. A. Brown and N. A. Jelley, J. of Phys. G8 (1982) 1699

35) M. El-Azab and G. R. Satchler, Nucl. Phys. A441 (1985) 157

36) P. Roussel, N. Alamanos, F. Auger, J. Barrette, B. Berthier, B. Fernandez, L. Papineau, H.

Doubre and W. Mitting, Phys. Rev. Lett. 54 (1985) 1779

37) S. Landowne and S. C. Pieper, Phys. Rev. C29 (1984) 1352

38) G. R. Satchler, M. A. Nagarajan, J. S. Lilley and I. J. Thompson, Ann. Phys. 178 (1987) 110

TABLE
Best folding fit parameters

E_{lab} (MeV)	N	W (MeV)	R_{1V} (fm)	a_{1V} (fm)	χ^2/n(Elastic)	Couplings	$R_s(V)$ (fm)	$R_s(W)$ (fm)
203.8	0.69 ± 0.06	50.0	8.38	0.848	1.8	0^+	11.1	12.0
	0.67 ± 0.08	50.0	9.65	0.546	0.7	0^+	11.1	12.1
		0.050	14.7	1.37*				
	0.83 ± 0.10	50.0	9.94	0.470	1.7	0^+2^+	11.1	11.8
	0.78 ± 0.12	50.0	9.94	0.466	1.7	$0^+2^+4^+$m.e.		
219.2	0.59 ± 0.10	50.0	9.61	0.561	3.0	0^+	11.3	12.1
	0.64 ± 0.06	50.0	9.85	0.491	1.5	0^+	11.3	12.2
		0.026	16.0	1.51*				
	1.00 ± 0.12	50.0	10.3	0.315	2.1	0^+2^+	11.2	11.6
	0.85 ± 0.14	50.0	10.3	0.324	2.8	$0^+2^+4^+$m.e.		

* Parameters on this row correspond to the imaginary surface term (see text)

ne astic scattering to higher levels is

Figure Captions

Fig. 1 Mass spectrum. The crosses indicate the expected position of the elastic and inelastic scattering events (+) and of the pick-up of one and two nucleons (×) in the ^{58}Ni+^{64}Ni interaction. Experimental level curves are drawn.

Fig. 2 Q-spectra corresponding to the whole set of events in fig. 1 (upper curve) or selecting those within the dashed contour (lower curve). Above the scattering spectrum are indicated the level schemes of ^{58}Ni and ^{64}Ni. Due to the differences between the Q-values of one-neutron pick-up (Q_{00} = −0.65 MeV) and of one-proton pick-up (Q_{00} = −9.13 MeV), the lower spectrum can be attributed to the former reaction.

Fig. 3 Comparison between elastic scattering data of this work (dots) and those of ref. [14]) (opened squares) measured at a slightly lower energy (203 MeV-lab). Also are compared the elastic plus inelastic data ($Q > -5$ MeV) of this work (solid line) with the same kind of data of ref. [13]) (triangles) measured at the same energy.

Fig. 4 Comparison between elastic scattering data and theoretical analyses: 1) Optical model analyses with renormalized M3Y-folding potential for the real part, either with a standard Woods-Saxon imaginary potential (long dashes) or with volume and surface imaginary potentials (short dashes). 2) Coupled-channels calculations including the first 2^+ levels of both nucleus (solid curves), see table.

Fig. 5 Comparison between elastic and inelastic scattering data and coupled-channels analyses. The results for two channel coupling (0^+2^+) are drawn with solid curves which are the same as in fig. 4. The results of the calculations including also the mutual 2+ excitation and the 4^+ excitations are drawn with dashed curves. The best fit of the inelastic scattering data that could be obtained with a real coupling alone (i.e. without imaginary coupling) is shown by the point-dashed curves.

Fig. 6 Influence of the different parts of the coupling in the calculated elastic and inelastic angular distributions at E_{lab} = 203.8 MeV. The solid curves are the same as in figures 4 and 5, they are calculated using all the couplings (Coulomb, nuclear and imaginary). For the other curves only one coupling was used, either Coulomb (dashed curve), nuclear (point-dashed) or imaginary (short-long dashed).

sca ering. e in ro uce opt into t ıe ECIS code [22]) which searches

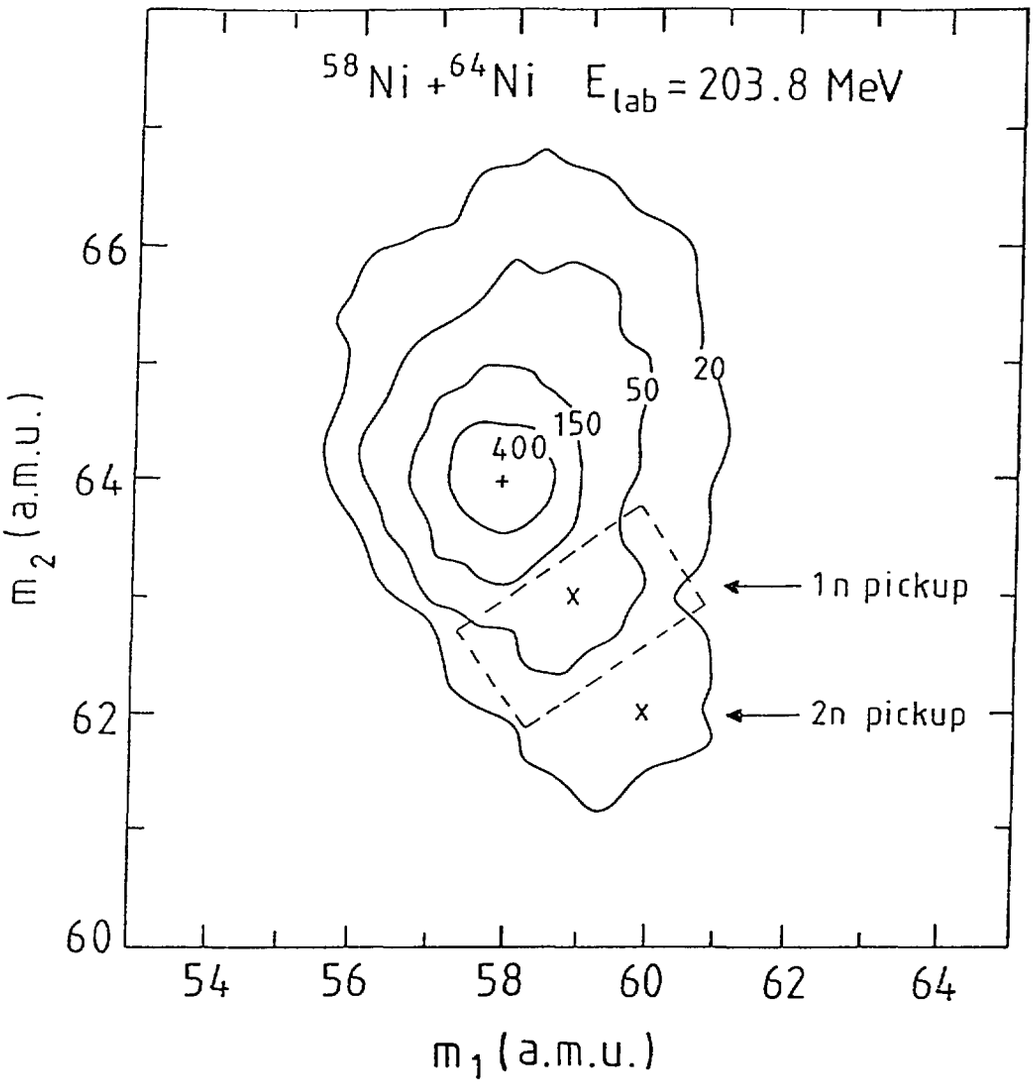

Fig. 1

s see s or - as ıe curves ın gure . t t e ug er energy

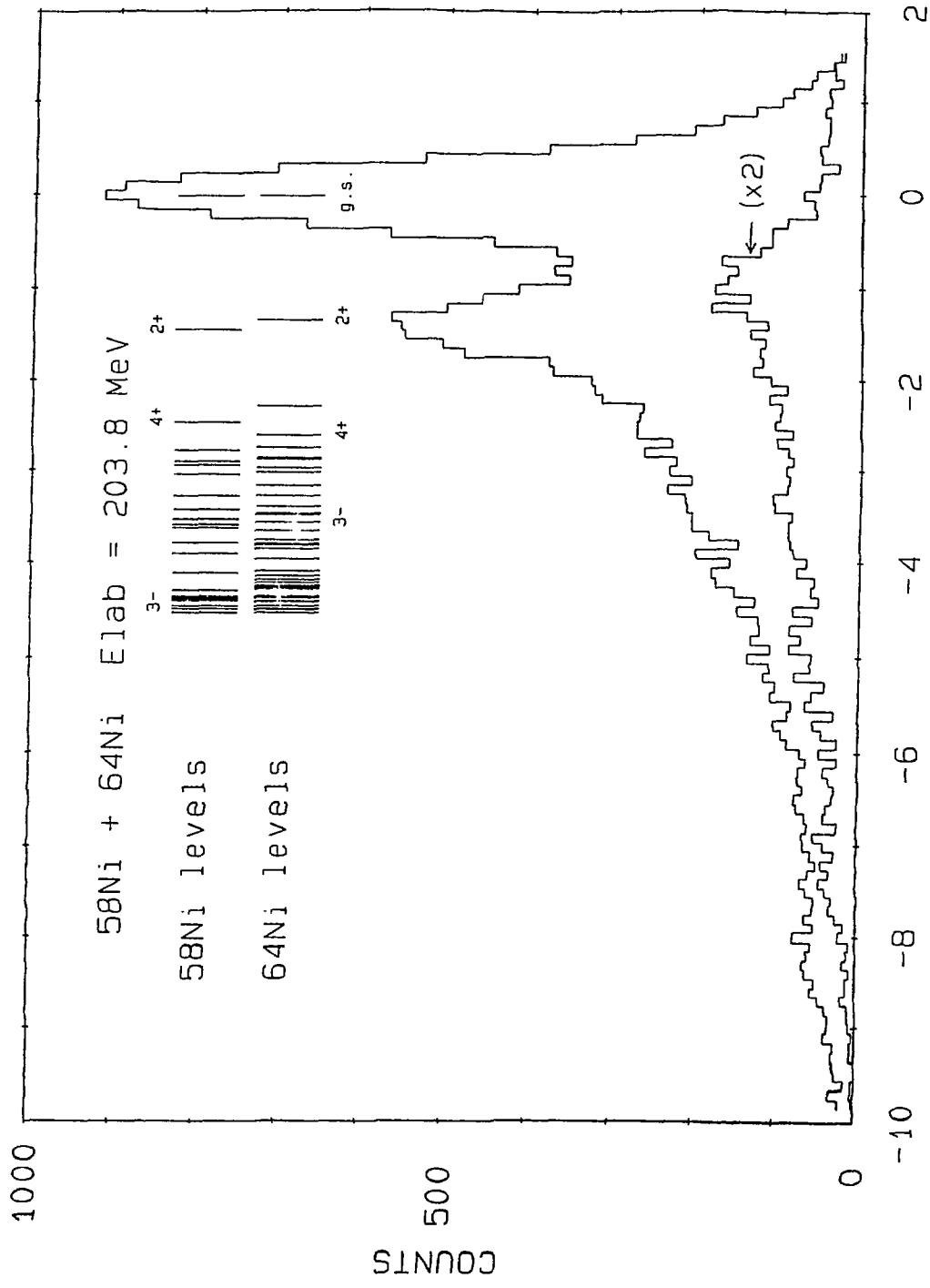

Fig. 2

the only difference is that for the coupling potentials one or both densities $\rho_i(r)$ are replaced by

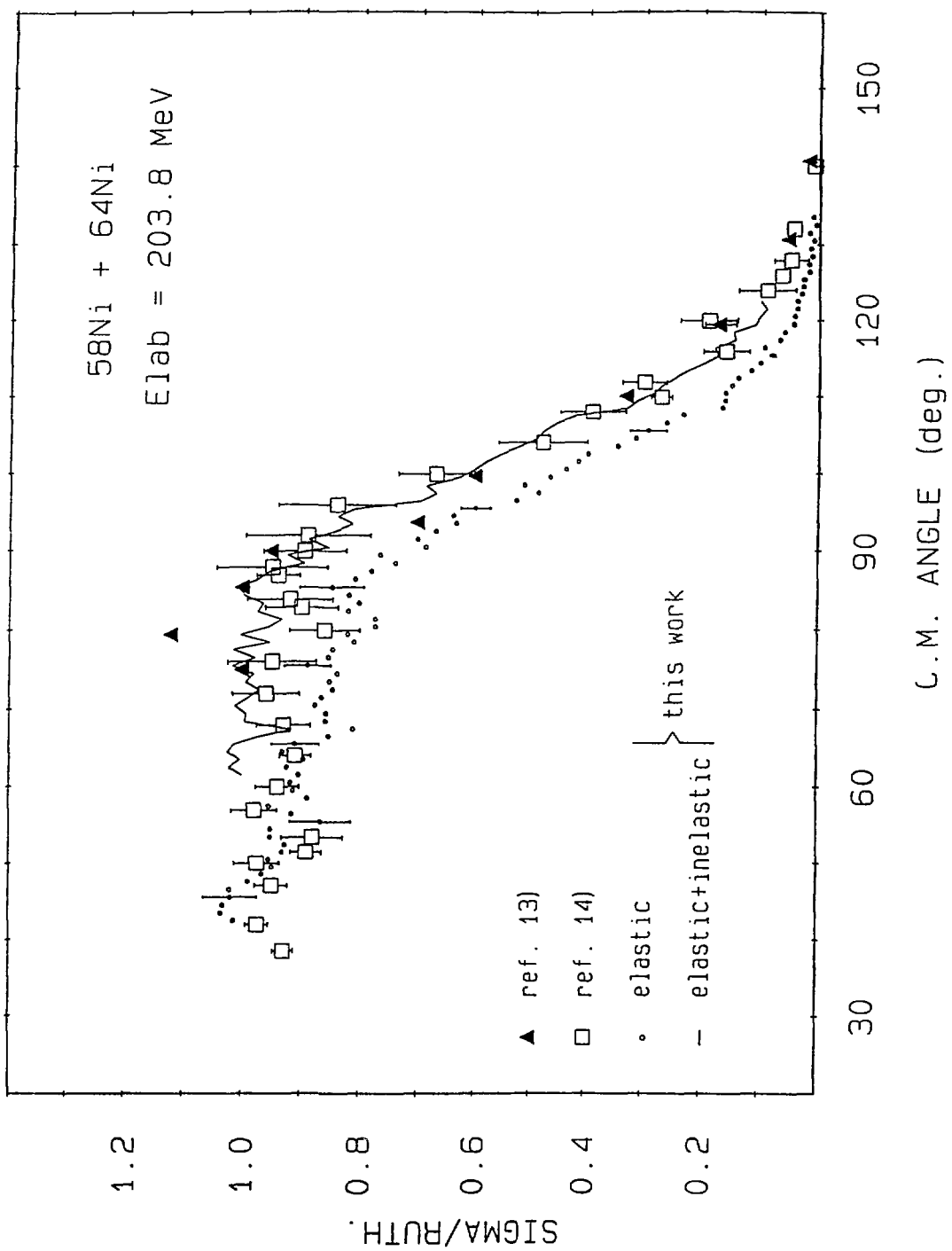

Fig. 3

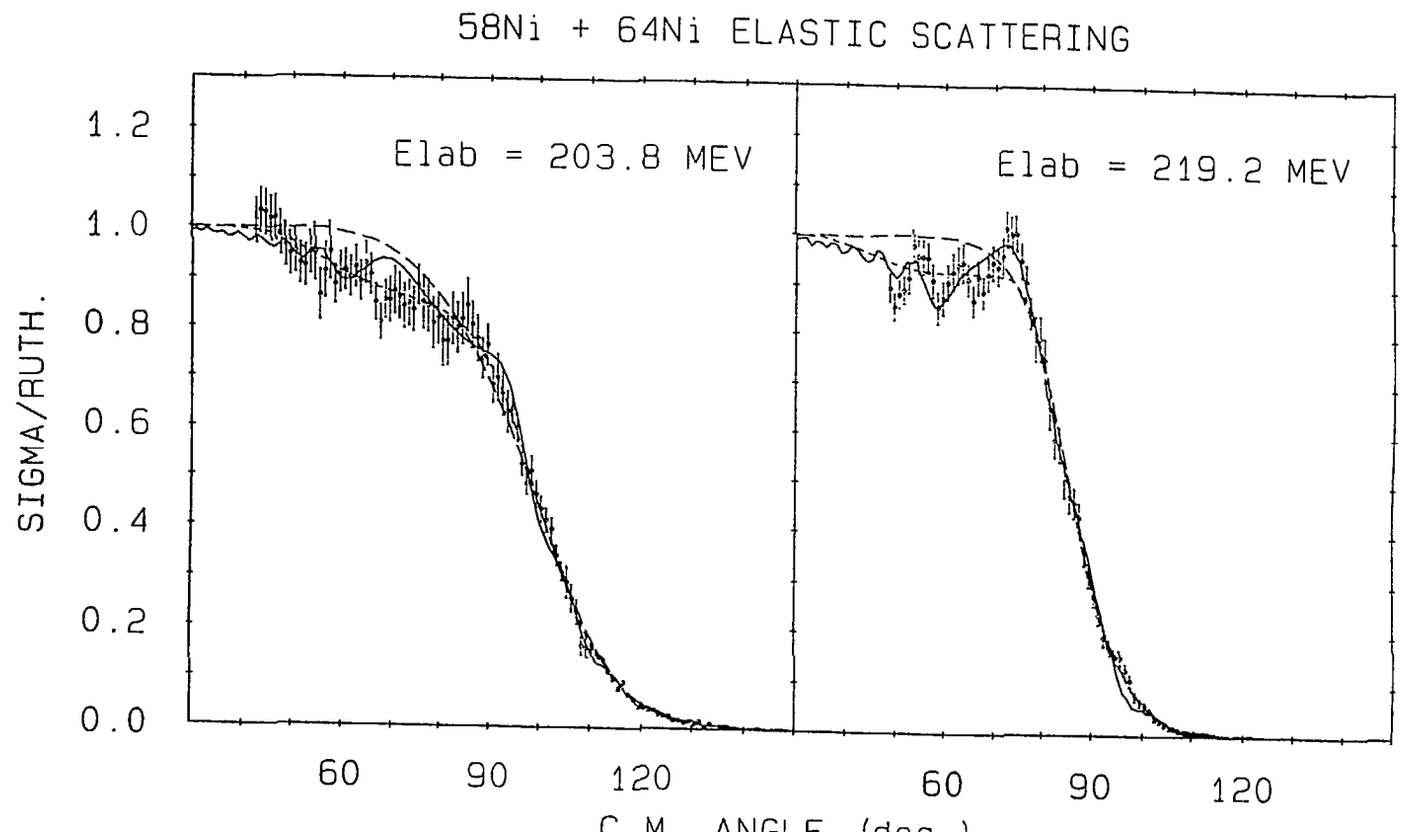
58Ni + 64Ni ELASTIC SCATTERING
Elab = 203.8 MEV
Elab = 219.2 MEV
SIGMA/RUTH.
1.2
1.0
0.8
0.6
0.4
0.2
0.0
60
90
120
60
90
120
C.M. ANGLE (deg.)

ecomposi ion o t e cross section at E_{lab} = 203.8 MeV. The inelastic scattering is dominated by

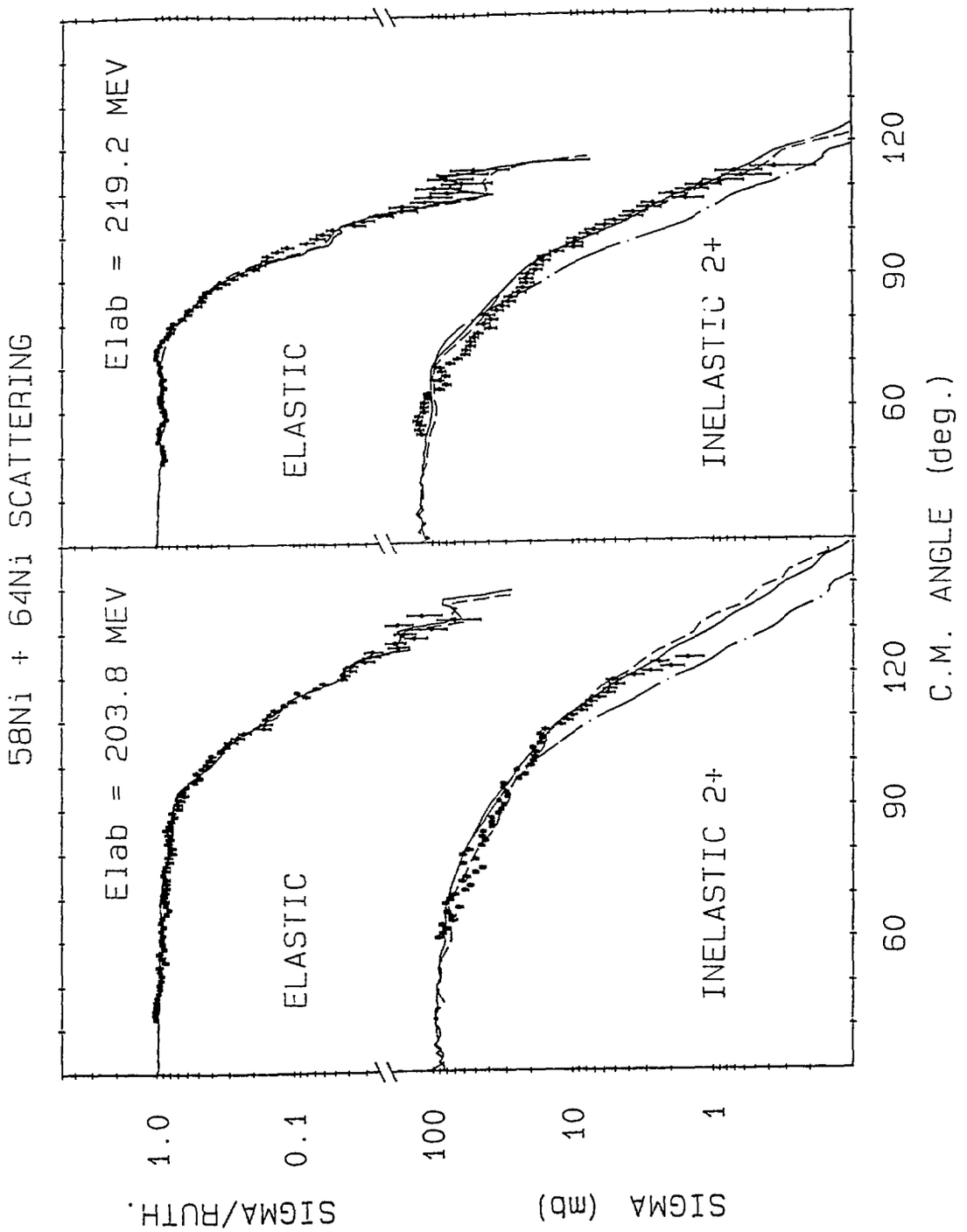

Fig. 5

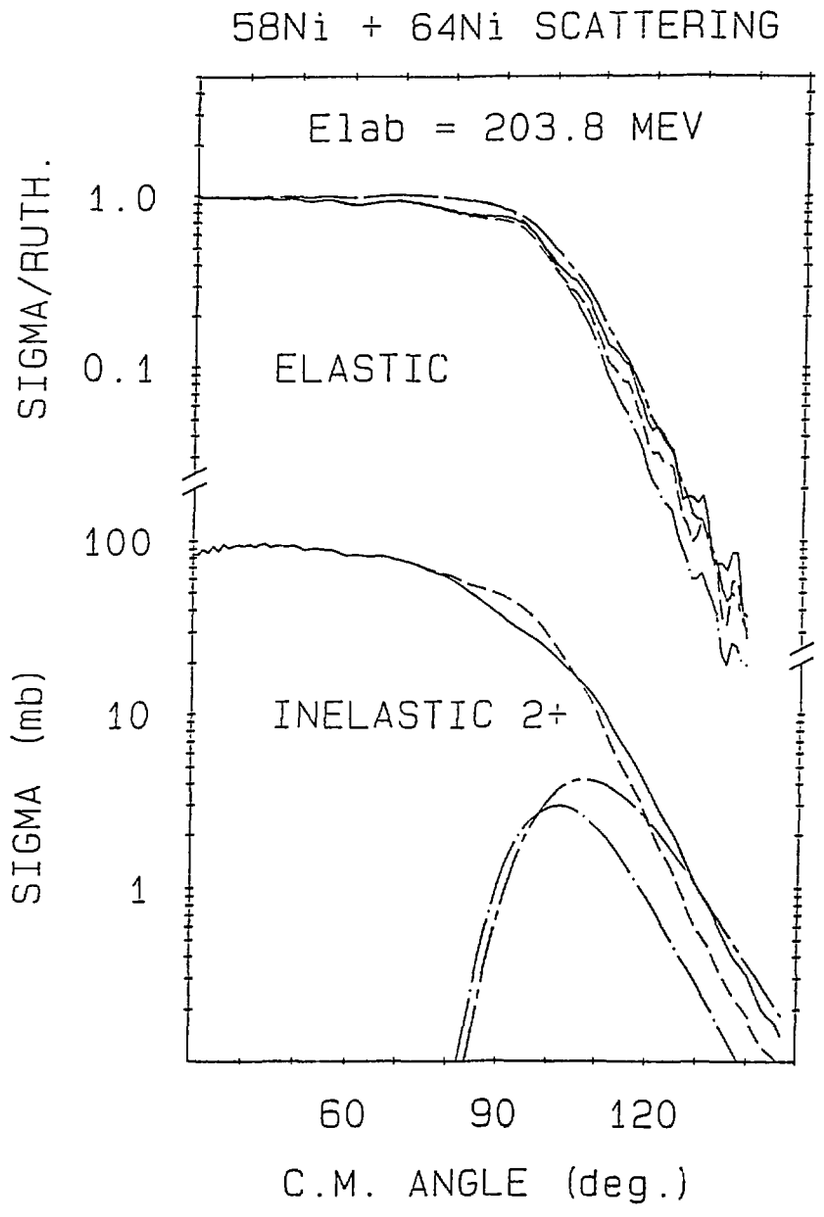
58Ni + 64Ni SCATTERING
Elab = 203.8 MEV
SIGMA/RUTH.
1.0
0.1
ELASTIC
100
10
INELASTIC 2+
SIGMA (mb)
1
60
90
120
C.M. ANGLE (deg.)

Fig. 6